Journal of Geo-Engineering Sciences 1 (2013) 53–67
DOI 10.3233/JGS-13007
IOS Press

A new framework for analysis of laterally loaded piles

Dipanjan Basu[a,*], Rodrigo Salgado[b] and Mônica Prezzi[b]
[a]*Department of Civil and Environmental Engineering, University of Waterloo, Waterloo, ON, Canada*
[b]*Department of Civil Engineering, Purdue University, West Lafayette, IN, USA*

Abstract. A new analysis framework is presented for calculation of the response of laterally loaded piles in multi-layered, heterogeneous elastic soil. The governing differential equations for the pile deflections in different soil layers are obtained using the principle of minimum potential energy after assuming a rational soil displacement field. Solutions for the pile deflection are obtained analytically, while those for the soil displacements are obtained using the finite difference method. The input parameters needed for the analysis are the pile geometry, soil profile and the elastic constants of the soil and pile. The method produces results with accuracy comparable to that of a three-dimensional finite element analysis but requires much less computation time. The analysis can take into account the spatial variation of soil properties along vertical, radial and tangential directions.

Keywords: Pile, analytical solution, lateral load, continuum approach, elastic analysis

1. Introduction

Piles are often subjected to lateral forces and moments arising due to wind, wave, traffic or seismic events. These external forces and moments are assumed to act at the pile head and the analysis is performed either by using the p-y method or by a continuum-based numerical method. In the p-y method, the lateral soil resistance is represented by a series of horizontal springs, which are attached to the pile segments into which the pile is discretized, and numerical methods are used to obtain the lateral displacements of the pile, which is assumed to behave as an Euler-Bernoulli beam [1–5]. The soil springs are characterized by the p-y curves, in which the resistive spring force p per unit pile length is given as a function of the lateral pile displacement y. Different p-y curves have been developed for different types of soils based mostly on field lateral pile load tests. The advantage of the p-y method is that the results are produced quickly, but available p-y curves are based on ad hoc assumptions and do not necessarily represent the actual soil resistance at a particular site. The continuum approach for the analysis of laterally-loaded piles is conceptually more robust than the p-y method. However, the complexity of a three-dimensional soil continuum often requires computationally expensive numerical techniques, such as the boundary element method or three-dimensional finite element analysis [6–11]. Consequently, continuum-based analyses are not typically used for design calculations.

In this paper, a continuum-based analysis framework is presented that produces results within a time frame comparable with that of the p-y method. Based on the assumption of a rational displacement field surrounding the

*Corresponding author: Dipanjan Basu, Assistant Professor, Department of Civil and Environmental Engineering, University of Waterloo, 200 University Avenue West, Waterloo, ON, N2L 3G1, Canada. E-mails: dipanjan.basu@uwaterloo.ca; rodrigo@purdue.edu (R. Salgado); mprezzi@purdue.edu (M. Prezzi).

ISSN 2213-2880/13/$27.50

pile, the framework integrates the three-dimensional soil resistance using the variational principles of mechanics. The three-dimensional soil resistance is then given as input to a one-dimensional pile analysis, and iterations are performed until equilibrium between the pile and soil are satisfied. The framework has several attractive features, which are demonstrated in this paper.

2. Analysis

2.1. Problem definition and scope

A single pile of circular cross section with radius r_p and length L_p is assumed to be embedded in a layered soil medium containing n layers (Fig. 1). The pile is elastic and behaves as an Euler-Bernoulli beam with a constant flexural rigidity E_pI_p. The layered continuum extends to infinity in all radial directions, and the bottom (n^{th}) layer extends to infinity downwards. The vertical depth to the base of any intermediate layer i is H_i, which implies that the thickness of the i^{th} layer is $H_i - H_{i-1}$ with $H_0 = 0$. The top (head) of the pile is at the level of the ground surface. The bottom (base) of the pile is embedded in the n^{th} layer. The soil layers are assumed to be elastic with Lame's constants λ_{si} and G_{si} for the i^{th} layer. Perfect contact between the pile and soil is assumed. A polar $(r - \theta - z)$ coordinate system is chosen with its origin coinciding with the pile head and the positive z-axis pointing downward and coinciding with the pile axis. The purpose of the analysis is to obtain pile deflection, bending moment and shear force as a function of the applied horizontal force F_a and moment M_a acting at the pile head.

2.2. Soil displacement, strain and stress

Each component of the displacement at any point within the soil continuum (Fig. 2) is assumed to be a product of separable functions [12]:

$$u_r = w(z)\,\phi_r(r)\,\cos\theta \tag{1a}$$

$$u_\theta = -w(z)\,\phi_\theta(r)\,\sin\theta \tag{1b}$$

$$u_z = 0 \tag{1c}$$

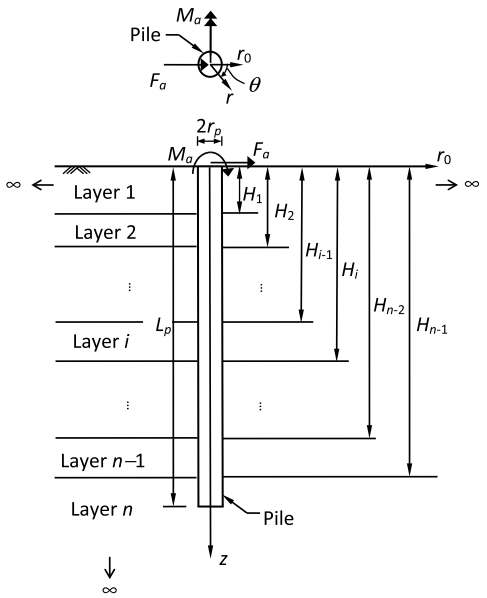

Fig. 1. Laterally loaded pile in layered soil media.

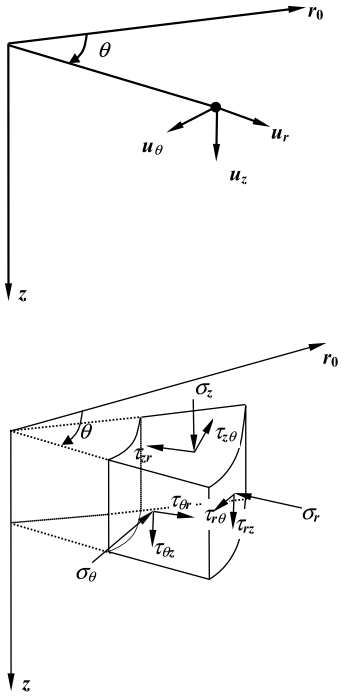

Fig. 2. (a) Displacements and (b) stresses within soil mass.

where $w(z)$ is a displacement function varying with depth z that describes the lateral deflection of the pile, $\phi_r(r)$ and $\phi_\theta(r)$ are dimensionless displacement functions varying with the radial coordinate r, and θ is measured counterclockwise from a vertical reference section ($r = r_0$) that contains the applied force vector F_a. It is reasonable to assume that the vertical displacement of the soil due to the lateral load and moment applied at the head of the pile is negligible; this justifies Equation (1c). The functions $\phi_r(r)$ and $\phi_\theta(r)$ describe how the displacements within the soil mass (due to pile deflection) decrease with increase in radial distance from the pile axis. It is assumed that $\phi_r(r) = 1$ and $\phi_\theta(r) = 1$ at $r = r_p$, which ensures perfect contact between the pile and soil at the interface, and that $\phi_r(r) = 0$ and $\phi_\theta(r) = 0$ as $r \longrightarrow \infty$, which ensures that the soil displacement due to pile movement decreases with increase in radial distance from the pile and becomes zero as the radial distance becomes large.

Using the above displacement field, the strains ε_{ij} within the soil can be expressed as:

$$\begin{bmatrix} \varepsilon_{rr} \\ \varepsilon_{\theta\theta} \\ \varepsilon_{zz} \\ \varepsilon_{r\theta} \\ \varepsilon_{rz} \\ \varepsilon_{\theta z} \end{bmatrix} = \begin{bmatrix} -\frac{\partial u_r}{\partial r} \\ -\frac{u_r}{r} - \frac{1}{r}\frac{\partial u_\theta}{\partial \theta} \\ -\frac{\partial u_z}{\partial z} \\ -\frac{1}{2}\left(\frac{1}{r}\frac{\partial u_r}{\partial \theta} + \frac{\partial u_\theta}{\partial r} - \frac{u_\theta}{r}\right) \\ -\frac{1}{2}\left(\frac{\partial u_z}{\partial r} + \frac{\partial u_r}{\partial z}\right) \\ -\frac{1}{2}\left(\frac{1}{r}\frac{\partial u_z}{\partial \theta} + \frac{\partial u_\theta}{\partial z}\right) \end{bmatrix} = \begin{bmatrix} -w(z)\frac{d\phi_r(r)}{dr}\cos\theta \\ -w(z)\frac{\phi_r(r)-\phi_\theta(r)}{r}\cos\theta \\ 0 \\ \frac{1}{2}w(z)\left\{\frac{\phi_r(r)-\phi_\theta(r)}{r} + \frac{d\phi_\theta(r)}{dr}\right\}\sin\theta \\ -\frac{1}{2}\frac{dw(z)}{dz}\phi_r(r)\cos\theta \\ \frac{1}{2}\frac{dw(z)}{dz}\phi_\theta(r)\sin\theta \end{bmatrix} \tag{2}$$

The strains can be related to stresses σ_{ij} using the elastic constitutive relationship:

$$\sigma_{ij} = \lambda_s \delta_{ij} \varepsilon_{kk} + 2G_s \varepsilon_{ij} \tag{3}$$

where δ_{ij} is the Kronecker's delta and summation is implied by repetition of indices.

2.3. Potential energy and its minimization

The total potential energy Π of the pile-soil system, including both the internal and external potential energies, is given by

$$\Pi = \frac{1}{2}E_pI_p\int_0^{L_p}\left(\frac{d^2w}{dz^2}\right)^2 dz + \int_0^{\infty}\int_0^{2\pi}\int_{r_p}^{\infty}\frac{1}{2}\sigma_{ij}\varepsilon_{ij}\, r\, dr\, d\theta\, dz$$

$$+\int_{L_p}^{\infty}\int_0^{2\pi}\int_0^{r_p}\frac{1}{2}\sigma_{ij}\varepsilon_{ij}\, r\, dr\, d\theta\, dz - F_a\, w|_{z=0} + M_a\left.\frac{dw}{dz}\right|_{z=0} \tag{4}$$

where w is the lateral pile deflection and σ_{ij} and ε_{ij} are the stress and strain tensors in the soil (Fig. 2). The first integral represents the internal potential energy of the pile. The second and the third integrals represent the internal potential energy of the soil continuum. The remaining two terms represent the external potential energy. The potential energy is minimized by setting its first variation equal to zero ($\delta\Pi = 0$) to obtain the equilibrium configuration of the pile-soil system. Considering the stress-strain-displacement relationships expressed in Equations (2) and (3), the potential energy density $\frac{1}{2}\sigma_{ij}\varepsilon_{ij}$ of the soil can be expressed in terms of the displacement functions and elastic constants. Substituting the expression of the potential energy density in Equation (4) and then setting $\delta\Pi = 0$ gives [13]

$$\begin{aligned}
&\int_0^{L_p} E_pI_p\frac{d^2w}{dz^2}\delta\left(\frac{d^2w}{dz^2}\right)dz + \int_0^{\infty}\int_{r_p}^{\infty}\int_0^{2\pi}\Bigg[(\lambda_s+2G_s)\, w\, \delta w\left(\frac{d\phi_r}{dr}\right)^2\cos^2\theta \\
&+(\lambda_s+2G_s)\, w^2\cos^2\theta\left(\frac{d\phi_r}{dr}\right)\delta\left(\frac{d\phi_r}{dr}\right) + 2\lambda_s w\,\delta w\cos^2\theta\frac{1}{r}\frac{d\phi_r}{dr}(\phi_r-\phi_\theta) \\
&+\lambda_s w^2\cos^2\theta\frac{1}{r}\frac{d\phi_r}{dr}\delta\phi_r - \lambda_s w^2\cos^2\theta\frac{1}{r}\frac{d\phi_r}{dr}\delta\phi_\theta \\
&+(\lambda_s+2G_s)\, w\,\delta w\cos^2\theta\frac{1}{r^2}(\phi_r-\phi_\theta)^2 + (\lambda_s+2G_s)\, w^2\cos^2\theta\frac{1}{r^2}(\phi_r-\phi_\theta)\delta\phi_r \\
&-(\lambda_s+2G_s)\, w^2\cos^2\theta\frac{1}{r^2}(\phi_r-\phi_\theta)\delta\phi_\theta + G_s w\,\delta w\sin^2\theta\frac{1}{r^2}\,(\phi_r-\phi_\theta)^2 \\
&+2G_s w\,\delta w\sin^2\theta\frac{1}{r}\frac{d\phi_\theta}{dr}(\phi_r-\phi_\theta) + G_s w^2\sin^2\theta\,\frac{1}{r^2}(\phi_r-\phi_\theta)\delta\phi_r \\
&-G_s w^2\sin^2\theta\,\frac{1}{r^2}(\phi_r-\phi_\theta)\delta\phi_\theta + G_s w^2\sin^2\theta\frac{1}{r}\frac{d\phi_\theta}{dr}\delta\phi_r - G_s w^2\sin^2\theta\frac{1}{r}\frac{d\phi_\theta}{dr}\delta\phi_\theta \\
&+G_s w\,\delta w\sin^2\theta\left(\frac{d\phi_\theta}{dr}\right)^2 + G_s w^2\sin^2\theta\frac{d\phi_\theta}{dr}\delta\left(\frac{d\phi_\theta}{dr}\right) \\
&+G_s w^2\sin^2\theta\frac{1}{r}(\phi_r-\phi_\theta)\,\delta\left(\frac{d\phi_\theta}{dr}\right) + G_s\frac{dw}{dz}\delta\left(\frac{dw}{dz}\right)\phi_r^2\cos^2\theta \\
&+G_s\left(\frac{dw}{dz}\right)^2\cos^2\theta\,\phi_r\delta\phi_r + G_s\frac{dw}{dz}\delta\left(\frac{dw}{dz}\right)\phi_\theta^2\sin^2\theta \\
&+G_s\left(\frac{dw}{dz}\right)^2\sin^2\theta\,\phi_\theta\delta\phi_\theta\Bigg]\, rd\theta drdz + \pi r_p^2G_s\int_{L_p}^{\infty}\frac{dw}{dz}\delta\left(\frac{dw}{dz}\right)dz \\
&-F_a\delta\, w|_{z=0} + M_a\delta\left(\frac{dw}{dz}\right)\Bigg|_{z=0} = 0
\end{aligned} \tag{5}$$

where the Lame's constants vary spatially within any soil layer (i.e., $\lambda_s = \lambda_s(r, \theta, z)$ and $G_s = G_s(r, \theta, z)$).

The above equation is of the form

$$\delta\Pi = \left\{ A(w)\,\delta w + B(w)\,\delta\left(\frac{dw}{dz}\right)\right\} + \{C(\phi_r)\,\delta\phi_r\} + \{D(\phi_\theta)\,\delta\phi_\theta\} = 0 \tag{6}$$

Since the variations $\delta w(z)$, $\delta(dw/dz)$, $\delta\phi_r(r)$ and $\delta\phi_\theta(r)$ of the functions $w(z)$ (and its derivative), $\phi_r(r)$ and $\phi_\theta(r)$ are independent, the terms associated with each of these variations must individually be equal to zero (i.e., $A(w)\,\delta w = 0$, $B(w)\,\delta\left(dw/dz\right) = 0$, $C(\phi_r)\,\delta\phi_r = 0$ and $D(\phi_\theta)\,\delta\phi_\theta = 0$) in order to satisfy the condition $\delta\Pi = 0$. The resulting equations produce the optimal functions $w_{\text{opt}}(z)$, $\phi_{r,\text{opt}}(r)$ and $\phi_{\theta,\text{opt}}(r)$ that describe the equilibrium configuration of the pile-soil system.

2.4. Soil displacement differential equations

We first consider the variation of $\phi_r(r)$. All the terms associated with $\delta\phi_r$ and $\delta\left(\frac{d\phi_r}{dr}\right)$ are collected from Equation (5) and their summation is equated to zero. This gives the following differential equation

$$\begin{aligned}&\frac{d^2\phi_r}{dr^2} + \frac{1}{m_{s1}}\frac{dm_{s1}}{dr}\frac{d\phi_r}{dr} - \left\{\frac{1}{r^2}\frac{m_{s1}+m_{s2}+m_{s3}}{m_{s1}} - \frac{1}{r}\frac{1}{m_{s1}}\frac{dm_{s3}}{dr} + \frac{n_{s1}}{m_{s1}}\right\}\phi_r \\ &\quad = \frac{m_{s2}+m_{s3}}{m_{s1}}\frac{1}{r}\frac{d\phi_\theta}{dr} - \left\{\frac{1}{r^2}\frac{m_{s1}+m_{s2}+m_{s3}}{m_{s1}} - \frac{1}{r}\frac{1}{m_{s1}}\frac{dm_{s3}}{dr}\right\}\phi_\theta\end{aligned} \tag{7}$$

with the boundary conditions $\phi_r = 1$ at $r = r_p$ and $\phi_r = 0$ at $r = \infty$. The terms in the above equation are given by

$$m_{s1}(r) = \int_0^\infty\int_0^{2\pi}(\lambda_s + 2G_s)w^2\cos^2\theta r d\theta dz = \sum_{i=1}^{n}\int_{H_{i-1}}^{H_i}\int_0^{2\pi}(\lambda_{si} + 2G_{si})w_i^2\cos^2\theta r d\theta dz \tag{8a}$$

$$m_{s2}(r) = \int_0^\infty\int_0^{2\pi}G_s w^2\sin^2\theta r d\theta dz = \sum_{i=1}^{n}\int_{H_{i-1}}^{H_i}\int_0^{2\pi}G_{si}w_i^2\sin^2\theta r d\theta dz \tag{8b}$$

$$m_{s3}(r) = \int_0^\infty\int_0^{2\pi}\lambda_s w^2\cos^2\theta r d\theta dz = \sum_{i=1}^{n}\int_{H_{i-1}}^{H_i}\int_0^{2\pi}\lambda_{si}w_i^2\cos^2\theta r d\theta dz \tag{8c}$$

$$n_{s1}(r) = \int_0^\infty\int_0^{2\pi}G_s\left(\frac{dw}{dz}\right)^2\cos^2\theta r d\theta dz = \sum_{i=1}^{n}\int_{H_{i-1}}^{H_i}\int_0^{2\pi}G_{si}\left(\frac{dw_i}{dz}\right)^2\cos^2\theta r d\theta dz \tag{8d}$$

In Equations (8a)–(8d), the subscript i represents the i^{th} layer of the multi-layered continuum; w_i represents the function $w(z)$ in the i^{th} layer with $w_i|_{z=H_i} = w_{i+1}|_{z=H_i}$; and $H_n = \infty$.

Next, the variation on $\phi_\theta(r)$ is considered. The terms containing $\delta\phi_\theta$ and $\delta\left(\frac{d\phi_\theta}{dr}\right)$ are collected from Equation (5) and equated to zero. Following a similar procedure as that for ϕ_r, the governing differential equation for ϕ_θ is obtained:

$$\begin{aligned}&\frac{d^2\phi_\theta}{dr^2} + \frac{1}{m_{s2}}\frac{dm_{s2}}{dr}\frac{d\phi_\theta}{dr} - \left\{\frac{1}{r^2}\frac{m_{s1}}{m_{s2}} + \frac{1}{r}\frac{1}{m_{s2}}\frac{dm_{s2}}{dr} + \frac{n_{s2}}{m_{s2}}\right\}\phi_\theta \\ &\quad = -\frac{m_{s2}+m_{s3}}{m_{s2}}\frac{1}{r}\frac{d\phi_r}{dr} - \left\{\frac{1}{r^2}\frac{m_{s1}}{m_{s2}} + \frac{1}{r}\frac{1}{m_{s2}}\frac{dm_{s2}}{dr}\right\}\phi_r\end{aligned} \tag{9}$$

with the boundary conditions that $\phi_\theta = 0$ at $r = \infty$ and $\phi_\theta = 1$ at $r = r_p$, where

$$n_{s2}(r) = \int_0^\infty \int_0^{2\pi} G_s \left(\frac{dw}{dz}\right)^2 \sin^2\theta r d\theta dz = \sum_{i=1}^{n} \int_{H_{i-1}}^{H_i} \int_0^{2\pi} G_{si} \left(\frac{dw_i}{dz}\right)^2 \sin^2\theta r d\theta dz \tag{8e}$$

The quantities $m_{s1}, m_{s2}, m_{s3}, n_{s1}$ and n_{s2} are obtained by numerical integrations performed along the tangential and vertical directions.

2.5. Pile displacement differential equations

Finally, the variation of w is considered. Referring back to Equation (5), the terms associated with δw and $\delta\left(\frac{dw}{dz}\right)$ are collected and their sum is equated to zero. Further, the domain is split into sub-domains $0 \le z \le H_1$, $H_1 \le z \le H_2, \ldots, H_{n-1} \le z \le L_p$ and $L_p \le z < \infty$ following the natural layering present in the assumed soil profile. As before, the n^{th} (bottom) layer is artificially split into two parts, with the part below the pile denoted by the subscript $n+1$. The differential equation for any layer i ($i = 1, 2, \ldots, n$) is obtained, after expressing it in terms of normalized depth $\tilde{z} = z/L_p$ and normalized pile displacement $\tilde{w} = w/L_p$, as:

$$\frac{d^4\tilde{w}_i}{d\tilde{z}^4} - 2\tilde{t}_i \frac{d^2\tilde{w}_i}{d\tilde{z}^2} + \tilde{k}_i \tilde{w}_i = 0 \tag{10}$$

where

$$\tilde{t}_i = \begin{cases} \frac{L_p^2}{2E_pI_p} \int_{r_p}^{\infty} \int_0^{2\pi} G_{si} \left(\phi_r^2 \cos^2\theta + \phi_\theta^2 \sin^2\theta\right) r d\theta dr; & i = 1,\ 2,\ ...,\ n \\ \frac{L_p^2}{2E_pI_p} \left(\int_{r_p}^{\infty} \int_0^{2\pi} G_{sn} \left(\phi_r^2 \cos^2\theta + \phi_\theta^2 \sin^2\theta\right) r d\theta dr + \pi G_{sn} r_p^2 \right); & i = n+1 \end{cases} \tag{11}$$

$$\begin{aligned} \tilde{k}_i = \frac{L_p^4}{E_pI_p} \int_{r_p}^{\infty} \int_0^{2\pi} \Bigg[& (\lambda_{si} + 2G_{si}) \left(\frac{d\phi_r}{dr}\right)^2 \cos^2\theta + 2\lambda_{si} \frac{1}{r} \frac{d\phi_r}{dr} (\phi_r - \phi_\theta) \cos^2\theta \\ & + (\lambda_{si} + 2G_{si}) \frac{1}{r^2} (\phi_r - \phi_\theta)^2 \cos^2\theta + G_{si} \frac{1}{r^2} (\phi_r - \phi_\theta)^2 \sin^2\theta \\ & + 2G_{si} \frac{1}{r} (\phi_r - \phi_\theta) \frac{d\phi_\theta}{dr} \sin^2\theta + G_{si} \left(\frac{d\phi_\theta}{dr}\right)^2 \sin^2\theta \Bigg] r d\theta dr; i = 1, 2, ..., n \end{aligned} \tag{12}$$

The soil parameters $\tilde{k}_i$ and $\tilde{t}_i$ are obtained by performing numerical integrations along the radial and tangential directions.

The boundary conditions obtained at the pile head ($z = \tilde{z} = 0$) are:

$$\tilde{w}_1 = \text{constant} \tag{13a}$$

or

$$\frac{d^3\tilde{w}_1}{d\tilde{z}^3} - 2\tilde{t}_1 \frac{d\tilde{w}_1}{d\tilde{z}} - \tilde{F}_a = 0 \tag{13b}$$

and

$$\frac{d\tilde{w}_1}{d\tilde{z}} = \text{constant} \tag{13c}$$

or

$$\frac{d^2\tilde{w}_1}{d\tilde{z}^2} - \tilde{M}_a = 0 \tag{13d}$$

At the interface between any two layers ($z = H_i$ or $\tilde{z} = \tilde{H}_i$), the boundary conditions are:

$$\tilde{w}_i = \tilde{w}_{i+1} \tag{14a}$$

$$\frac{d\tilde{w}_i}{d\tilde{z}} = \frac{d\tilde{w}_{i+1}}{d\tilde{z}} \tag{14b}$$

$$\frac{d^3\tilde{w}_i}{d\tilde{z}^3} - 2\tilde{t}_i\frac{d\tilde{w}_i}{d\tilde{z}} = \frac{d^3\tilde{w}_{i+1}}{d\tilde{z}^3} - 2\tilde{t}_{i+1}\frac{d\tilde{w}_{i+1}}{d\tilde{z}} \tag{14c}$$

$$\frac{d^2\tilde{w}_i}{d\tilde{z}^2} = \frac{d^2\tilde{w}_{i+1}}{d\tilde{z}^2} \tag{14d}$$

At the pile base ($z = L_p$ or $\tilde{z} = 1$), the boundary conditions are:

$$\tilde{w}_n = \text{constant} \tag{15a}$$

or

$$\frac{d^3\tilde{w}_n}{d\tilde{z}^3} - 2\tilde{t}_n\frac{d\tilde{w}_n}{d\tilde{z}} - \sqrt{2\tilde{k}_n\tilde{t}_{n+1}}\,\tilde{w}_n = 0 \tag{15b}$$

and

$$\frac{d\tilde{w}_n}{d\tilde{z}} = \text{constant} \tag{15c}$$

or

$$\frac{d^2\tilde{w}_n}{d\tilde{z}^2} = 0 \tag{15d}$$

The dimensionless terms in the above equations are defined as: $\tilde{F}_a = \frac{F_a L_p^2}{E_p I_p}$, $\tilde{M}_a = \frac{M_a L_p}{E_p I_p}$ and $\tilde{H}_i = \frac{H_i}{L_p}$.

2.6. Solution of pile displacement differential equations

The general solution of Equation (10) is given by:

$$\tilde{w}_i(\tilde{z}) = C_1^{(i)}\Phi_1 + C_2^{(i)}\Phi_2 + C_3^{(i)}\Phi_3 + C_4^{(i)}\Phi_4 \tag{17}$$

where, $C_1^{(i)}$, $C_2^{(i)}$, $C_3^{(i)}$and $C_4^{(i)}$ are integration constants (for the i^{th} layer), and Φ_1, Φ_2, Φ_3 and Φ_4 are individual solutions (functions of $\tilde{z}$) of the differential equation. The functions Φ_1, Φ_2, Φ_3 and Φ_4 are standard trigonometric or hyperbolic functions that arise in the solution of the linear ordinary differential equations (Table 1). The integration constants for each layer can be determined using the boundary conditions described in Equations (13)–(15) [14, 15]. Once the pile displacement is obtained, the pile bending moment and shear force can also be obtained as functions of depth by appropriately differentiating the pile displacement with respect to depth.

2.7. Solution of soil displacement differential equations

The differential Equations (7) and (9) for ϕ_r and ϕ_θ are interdependent and are solved by the finite difference method. Considering a radially outward one-dimensional finite difference grid and using the central-difference scheme, Equations (7) and (9) are respectively written as:

Table 1
Functions in Equation (17)

Relative Magnitudes of $\tilde{k}$ and $\tilde{t}$	Constants a and b		Functions and Their Derivatives	Individual Solutions of Equation (10)			
	a	b		Φ_1	Φ_2	Φ_3	Φ_4
$\tilde{k} > \tilde{t}^2$	$\sqrt{\{1/2(\sqrt{\tilde{k}} + \tilde{t})\}}$	$\sqrt{\{1/2(\sqrt{\tilde{k}} - \tilde{t})\}}$	Φ	$\sinh a\tilde{z} \cos b\tilde{z}$	$\cosh a\tilde{z} \cos b\tilde{z}$	$\cosh a\tilde{z} \sin b\tilde{z}$	$\sinh a\tilde{z} \sin b\tilde{z}$
			Φ'	$a\Phi_2 - b\Phi_4$	$a\Phi_1 - b\Phi_3$	$a\Phi_4 + b\Phi_2$	$a\Phi_3 + b\Phi_1$
			Φ''	$\left(a^2 - b^2\right)\Phi_1 - 2ab\Phi_3$	$\left(a^2 - b^2\right)\Phi_2 - 2ab\Phi_4$	$\left(a^2 - b^2\right)\Phi_3 + 2ab\Phi_1$	$\left(a^2 - b^2\right)\Phi_4 + 2ab\Phi_2$
			Φ'''	$a\left(a^2 - 3b^2\right)\Phi_2 + b\left(b^2 - 3a^2\right)\Phi_4$	$a\left(a^2 - 3b^2\right)\Phi_1 + b\left(b^2 - 3a^2\right)\Phi_3$	$a\left(a^2 - 3b^2\right)\Phi_4 - b\left(b^2 - 3a^2\right)\Phi_2$	$a\left(a^2 - 3b^2\right)\Phi_3 - b\left(b^2 - 3a^2\right)\Phi_1$
$\tilde{k} < \tilde{t}^2$	$\sqrt{\{\tilde{t} + \sqrt{(\tilde{t}^2 - \tilde{k})}\}}$	$\sqrt{\{\tilde{t} - \sqrt{(\tilde{t}^2 - \tilde{k})}\}}$	Φ	$\sinh a\tilde{z}$	$\cosh a\tilde{z}$	$\sinh b\tilde{z}$	$\cosh b\tilde{z}$
			Φ'	$a\Phi_2$	$a\Phi_1$	$b\Phi_4$	$b\Phi_3$
			Φ''	$a^2\Phi_1$	$a^2\Phi_2$	$b^2\Phi_3$	$b^2\Phi_4$
			Φ'''	$a^3\Phi_2$	$a^3\Phi_1$	$b^3\Phi_4$	$b^3\Phi_3$

$$\frac{\phi_r^{j+1}-2\phi_r^j+\phi_r^{j-1}}{\Delta r^2}+\frac{1}{m_{s1}^j}\frac{m_{s1}^{j+1}-m_{s1}^{j-1}}{2\Delta r}\frac{\phi_r^{j+1}-\phi_r^{j-1}}{2\Delta r}-\left[\frac{1}{r_j^2}\frac{m_{s1}^j+m_{s2}^j+m_{s3}^j}{m_{s1}^j}-\frac{1}{r_j}\frac{1}{m_{s1}^j}\frac{m_{s3}^{j+1}-m_{s3}^{j-1}}{2\Delta r}+\frac{n_{s1}^j}{m_{s1}^j}\right]\phi_r^j=\frac{m_{s2}^j+m_{s3}^j}{m_{s1}^j}\frac{1}{r_j}\frac{\phi_\theta^{j+1}-\phi_\theta^{j-1}}{2\Delta r}-\left[\frac{1}{r_j^2}\frac{m_{s1}^j+m_{s2}^j+m_{s3}^j}{m_{s1}^j}-\frac{1}{r_j}\frac{1}{m_{s1}^j}\frac{m_{s3}^{j+1}-m_{s3}^{j-1}}{2\Delta r}\right]\phi_\theta^j \tag{17}$$

$$\frac{\phi_\theta^{j+1}-2\phi_\theta^j+\phi_\theta^{j-1}}{\Delta r^2}+\frac{1}{m_{s2}^j}\frac{m_{s2}^{j+1}-m_{s2}^{j-1}}{2\Delta r}\frac{\phi_\theta^{j+1}-\phi_\theta^{j-1}}{2\Delta r}-\left[\frac{1}{r_j^2}\frac{m_{s1}^j}{m_{s2}^j}+\frac{1}{r_j}\frac{1}{m_{s2}^j}\frac{m_{s2}^{j+1}-m_{s2}^{j-1}}{2\Delta r}+\frac{n_{s2}^j}{m_{s2}^j}\right]\phi_\theta^j=-\frac{m_{s2}^j+m_{s3}^j}{m_{s2}^j}\frac{1}{r_j}\frac{\phi_r^{j+1}-\phi_r^{j-1}}{2\Delta r}-\left[\frac{1}{r_j^2}\frac{m_{s1}^j}{m_{s2}^j}+\frac{1}{r_j}\frac{1}{m_{s2}^j}\frac{m_{s2}^{j+1}-m_{s2}^{j-1}}{2\Delta r}\right]\phi_r^j \tag{18}$$

where the superscript j represents the j^{th} node of the finite difference grid that is located at a distance of r_j from the pile-soil interface, and Δr is the radial distance between adjacent nodes.

Since the right-hand side of Equation (17) contains ϕ_θ, and the right-hand side of Equation (18) contains ϕ_r, iterations are necessary to obtain their values. An initial estimate of ϕ_r^j is made and given as input to Equation (18), and ϕ_θ^j is determined. The calculated ϕ_θ^j values are then given as input to Equation (17) to obtain ϕ_r^j. The newly obtained values of ϕ_r^j are again used to obtain new values of ϕ_θ^j, and the iterations are continued until convergence is reached. The criteria $\frac{1}{m}\sum_{j=1}^{m}\left|\phi_r^{j\text{previous}}-\phi_r^{j\text{current}}\right|\le 10^{-6}$and $\frac{1}{m}\sum_{j=1}^{m}\left|\phi_\theta^{j\text{previous}}-\phi_\theta^{j\text{current}}\right|\le 10^{-6}$, where m is the total number of nodes in the finite difference grid, are used to ensure that accurate values of ϕ_r and ϕ_θ are obtained (a stringent value of 10^{-6} is used because this iterative solution scheme is central to another set of iterations described next).

2.8. *Interdependence and iterative solutions of pile and soil displacements*

It is evident from Equations (11) and (12) that the functions $\phi_r(r)$ and $\phi_\theta(r)$ need to be known to estimate the parameters $\tilde{k}_i$ and $\tilde{t}_i$. This means that pile deflection cannot be obtained unless $\phi_r(r)$ and $\phi_\theta(r)$ are determined. Determination of $\phi_r(r)$ and $\phi_\theta(r)$ requires prior knowledge of the quantities m_{s1}, m_{s2}, m_{s3}, n_{s1} and n_{s2}, which, in turn, depend on the pile deflection w and slope $\frac{dw}{dz}$. Therefore, the pile-deflection and the soil-displacement equations are coupled and must be solved simultaneously using an iterative scheme (note that this iteration is separate from the ϕ-iterations described before).

In order to solve the coupled equations, trial profiles for ϕ_r and ϕ_θ are assumed and the values of $\tilde{t}_i$ and $\tilde{k}_i$ are obtained from Equations (11) and (12) using numerical integration. Pile deflection is then obtained, and m_{s1}, m_{s2}, m_{s3}, n_{s1} and n_{s2} are determined once the pile deflections are known. Using the calculated values of m_{s1}, m_{s2}, m_{s3}, n_{s1} and n_{s2}, ϕ_r and ϕ_θ are calculated by solving Equations (7) and (9) (using ϕ-iterations). The newly obtained profiles of ϕ_r and ϕ_θ are then compared with the previous (trial) profiles. If the differences are within the tolerable limits of $\frac{1}{m}\sum_{j=1}^{m}\left|\phi_r^{j\text{previous}}-\phi_r^{j\text{current}}\right|\le 10^{-3}$ and $\frac{1}{m}\sum_{j=1}^{m}\left|\phi_\theta^{j\text{previous}}-\phi_\theta^{j\text{current}}\right|\le 10^{-3}$ then the newly obtained ϕ_r and ϕ_θ and the corresponding w are accepted as the final solutions (note that the convergence criterion of 10^{-3} is different from the convergence criterion of 10^{-6} used for the ϕ-iterations described before). However, if the differences are greater than the tolerable limits, then the newly obtained profiles of ϕ_r and ϕ_θ are assumed to be the new trial profiles for the next iteration and the process is repeated until convergence on both ϕ_r and ϕ_θ is achieved.

3. Results

In this section, we illustrate some of the attractive features of the new analysis framework. First, the accuracy of the analysis is verified by comparing the results obtained by this analysis with those of equivalent three-dimensional (3D) finite element (FE) analysis. For the first example, a 15-m-long drilled shaft, with a diameter of 0.6 m and pile modulus $E_p = 24 \times 10^6$ kN/m^2, is considered embedded in a four-layer soil deposit with $H_1 = 2.0$ m, $H_2 = 5.0$ m and $H_3 = 8.3$ m; $E_{s1} = 20$ MPa, $E_{s2} = 35$ MPa, $E_{s3} = 50$ MPa and $E_{s4} = 80$ MPa; $\upsilon_{s1} = 0.35$, $\upsilon_{s2} = 0.25$, $\upsilon_{s3} = 0.2$ and $\upsilon_{s4} = 0.15$ (E_{si} and υ_{si} are the soil Young's modulus and Poisson's ratio for the i^{th} layer; E_{si} and υ_{si} are related to λ_{si} and G_{si} by $\lambda_{si} = E_{si}\upsilon_{si}/(1+\upsilon_{si})(1-2\upsilon_{si})$ and $G_{si} = E_{si}/2(1+\upsilon_{si})$). A horizontal force $F_a = 300$ kN acts at the pile head. The pile head and base are free to deflect and rotate. Figure 3 shows the pile deflection profile obtained using the present analysis and a 3D FE analysis. The FE analysis was performed using Abaqus with the assumption that the pile and soil behave as linear-elastic materials. The pile response obtained from the present analysis closely matches that of 3D FE analysis.

The second example consists of a 40-m long, 1.7-m diameter drilled shaft with $E_p = 25 \times 10^6$ kPa embedded in a four-layer soil profile with $H_1 = 1.5$ m, $H_2 = 3.5$ m, and $H_3 = 8.5$ m; $E_{s1} = 20$ MPa, $E_{s2} = 25$ MPa, $E_{s3} = 40$ MPa and $E_{s4} = 80$ MPa; $\upsilon_{s1} = 0.35$, $\upsilon_{s2} = 0.3$, $\upsilon_{s3} = 0.25$ and $\upsilon_{s4} = 0.2$. A 3000 kN force acts at the pile head, which is free to deflect and rotate. Figure 4 shows the pile deflection profiles, as obtained from the present analysis and 3D linear-elastic FE analysis performed using Abaqus. As before, the results from both analyses match quite closely.

The above examples not only show that the developed framework can predict pile deflection with an accuracy comparable to that of 3D FE analysis, but also illustrate that the framework takes into account discrete soil layering quite efficiently. In fact, a gradual variation of soil modulus with depth can also be taken into account by assuming multiple thin soil layers. As an example, the 15-m long pile described above, subjected to a horizontal load of 300 kN, is assumed to be embedded in a two-layer soil profile with the top layer extending down to 10 m and underlain by a stronger layer that goes down to great depth. The Young's modulus in the top layer increases from 10 MPa at the surface to 50 MPa at the depth of 10 m. The second layer is relatively homogeneous with Young's modulus equal to 100 MPa. The Poisson's ratio of the top layer can be assumed to be spatially constant at 0.4 while that of the second layer is 0.25. The problem is analyzed by dividing the top layer into 50 sub-layers of 0.2 m thickness. Figure 5 shows the pile deflection profile. The same problem is analyzed again with an average value of Young's modulus equal to 30 MPa for the top layer (calculated at the center of the layer) that remains spatially constant with depth, and the resulting pile deflection is plotted in Figure 5 as well. The figure shows that there can be significant error in pile response if averaging of soil properties is done naively over large depths. Figure 5 also shows the flexibility of the analysis framework in incorporating different possible variations of soil modulus, either continuous or discrete, with depth.

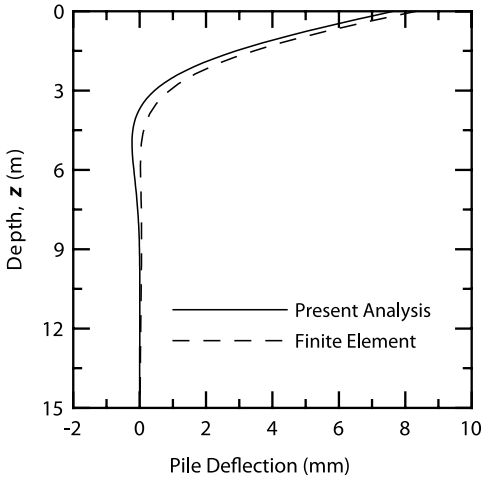

Fig. 3. Comparison of pile deflection profiles obtained from the present analysis and finite element analysis for a 15-m long pile.

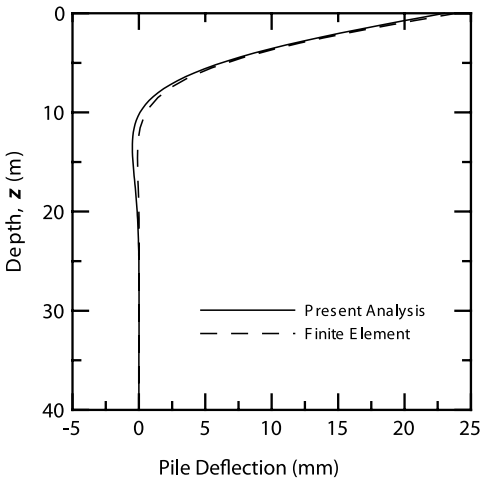

Fig. 4. Comparison of pile deflection profiles obtained from the present analysis and finite element analysis for a 40-m long pile.

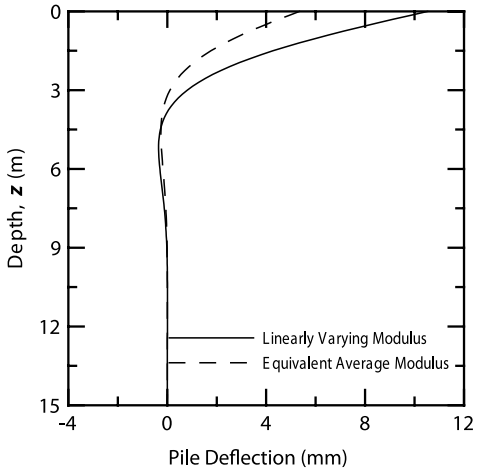

Fig. 5. Deflection profile for a 15-m long pile in a two-layer soil profile with modulus increasing linearly with depth in the top layer.

The analysis framework can not only incorporate variations of soil modulus with depth but also take into account spatial variations of soil modulus in the horizontal direction. Variation of soil properties in the horizontal direction can be due to the natural variability of a deposit, due to disturbance caused by pile installation or due to other reasons. For driven piles, the soil surrounding the pile is severely disturbed due to pile installation effects and the properties immediately adjacent to the pile are altered significantly from their *in situ* values. In some deposits, the modulus value adjacent to the pile becomes less than the *in situ* value while, in other deposits, the modulus value may increase due to soil densification. In order to demonstrate that the analysis can take into account the pile installation effects and variation of soil modulus along radial directions, the two examples of 15-m and 40-m long piles embedded in four-layer soil profiles, as described above, are considered again. First, it is assumed that the soil Young's moduli E_s of all the four layers reduce to a fraction f_r of their *in situ* values at the pile-soil interface (Case 1). Subsequently, it is assumed that the Young's moduli of all the four layers at the pile soil interface increase to values that are m_l times their *in situ* values (Case 2). In both the cases, it is assumed that the Young's moduli vary

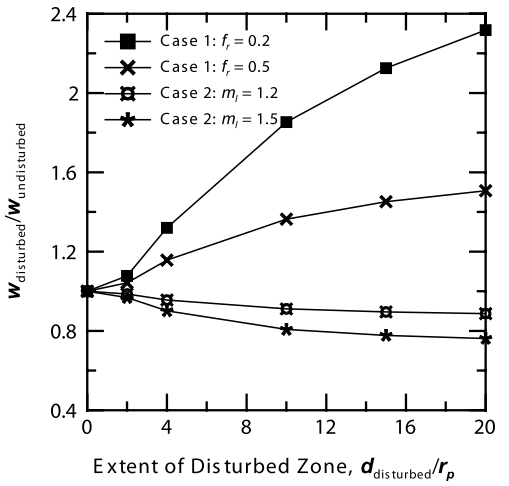

Fig. 6. Effect of pile installation on the lateral response of the 15-m long pile of example 1: for case 1,the soil Young's modulus increases radially from a fraction f_r of the *in situ* value at the pile-soil interface to the original *in situ* value at a radial distance $d_{\text{disturbed}}$ measured from the pile-soil interface; for case 2, the soilYoung's modulus decreases radially from a multiple m_l of the *in situ* value at the pile-soil interface to the original *in situ* value at a radial distance $d_{\text{disturbed}}$ measured from the pile-soil interface.

linearly in the radial directions from their altered values at the pile-soil interface to their original *in situ* values at a radial distance $d_{\text{disturbed}}$ measured from the pile-soil interface. At radial distances greater than $d_{\text{disturbed}}$ from the pile-soil interface, the moduli remain spatially constant at their *in situ* values. It is further assumed that the Poisson's ratios of the soil layers are not altered by the pile installation and remain spatially constant.

Figures 6 and 7 show the pile head deflection $w_{\text{disturbed}}$ for 15-m and 40-m piles, respectively, obtained for soil disturbance cases 1 and 2 described above, normalized with respect to the head deflection $w_{\text{undisturbed}}$ obtained for the corresponding cases without considering soil disturbance, as a function of the radial extent $d_{\text{disturbed}}$ of the disturbed soil zone normalized with respect to the pile radius r_p. For case 1, $f_r = 0.2$ and 0.5 are assumed for the simulations with $d_{\text{disturbed}}/r_p$ spanning over a range 2.0–20.0. For case 2, $m_l = 1.2$ and 1.5, and $d_{\text{disturbed}}/r_p =$ 2.0–20.0 are assumed. It is observed that both the magnitude of change in soil modulus and the extent of the disturbed zone impact the lateral pile response. It is interesting to note that the ratio $w_{\text{disturbed}}/w_{\text{undisturbed}}$ for both the piles are almost the same for identical values of f_r or m_l and $d_{\text{disturbed}}/r_p$.

The analysis can also capture the tangential (circumferential) variation of soil modulus. In the problem of laterally loaded piles, the soil in front of the loaded pile (i.e., the zone of soil for which $270^\circ \leq \theta \leq 90^\circ$) is compressed as the pile pushes against it. The soil behind the pile (i.e., the zone covered by $90^\circ \leq \theta \leq 270^\circ$) experiences a stress release and sometimes there is a lack of contact between the pile and the soil at the back. The change in the confining stress in soil due to pile movement may alter the stiffness as compression may dominate over shearing. Therefore, the soil modulus may vary as a function of θ. A simple way of taking into account this variation of soil modulus is by assigning different values of soil modulus in front of and behind the pile. As an illustration, the same examples of 15-m and 40-m piles described above are considered with the assumption that the Young's modulus of soil in front of the pile increases by 50% from the *in situ* value while it decreases by 50% and 100% at the back of the pile (a 100% decrease in the modulus approximately represents the case where there is a loss of contact between the pile and soil). This change in the circumferential variation of soil modulus is restricted to a depth of 1.5 m from the ground surface for the 15-m long pile and to a depth of 4 m from the ground surface for the 40-m long pile within which the effect of lateral pile movement on the soil modulus is likely to be most predominant (see Figs. 3 and 4). The Poisson's ratio of the soil layers are assumed to be not affected by the pile movement. Figures 8 and 9 show the deflection profiles for the 15-m and 40-m piles, respectively. The figures illustrate the ability of the analysis to consider the tangential variation of soil modulus and show that the change in modulus in front of and behind the pile affects the pile response.

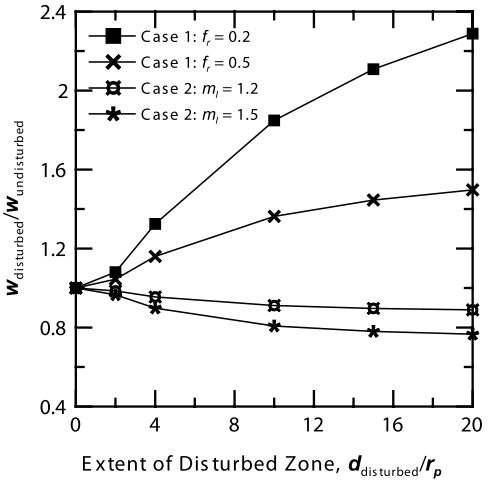

Fig. 7. Effect of pile installation on the lateral response of the 40-m long pile of example 2: for case 1, the soil Young's modulus increases radially from a fraction f_r of the *in situ* value at the pile-soil interface to the original *in situ* value at a radial distance $d_{\text{disturbed}}$ measured from the pile-soil interface; for case 2, the soil Young's modulus decreases radially from a multiple m_l of the *in situ* value at the pile-soil interface to the original *in situ* value at a radial distance $d_{\text{disturbed}}$ measured from the pile-soil interface.

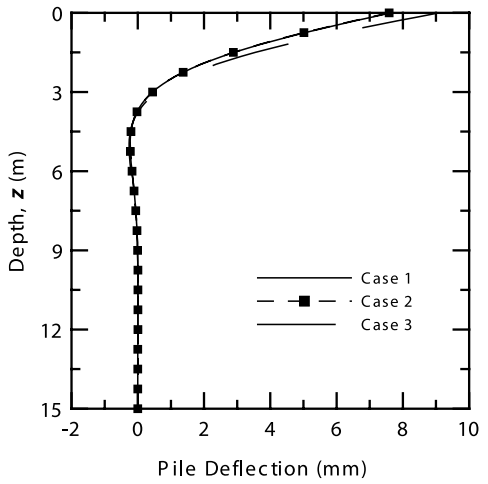

Fig. 8. Effect of varying soil modulus in front and back of a 15-m long pile on its lateral response: for case 1, the soil modulus is the same in the front and back of pile; for case 2, in the top 1.5 m, the soil modulus increases by 50% from the *in situ* value in the front of the pile and decreases by 50% from the *in situ* value at the back of the pile; for case 3, in the top 1.5 m, the soil modulus increases by 50% from the *in situ* value in front of the pile and the soil loses contact with the pile at the back.

It is important to note that the inputs required for the analysis — the pile radius and length, thicknesses of the soil layers, Young's modulus of the pile material, the elastic constants of the soil in the various layers, and the magnitudes of the applied force and moment — is given to the computer code in a text file. Thus, unlike finite element software, no specialized skills are required to run the computer code for this analysis. Further, the results of the analysis presented in this paper were obtained in less than three minutes by running the computer code in a Windows based laptop computer with 1.6 GHz processor and 4 GB RAM. This is significantly faster than the time required to run an equivalent 3D FE analysis.

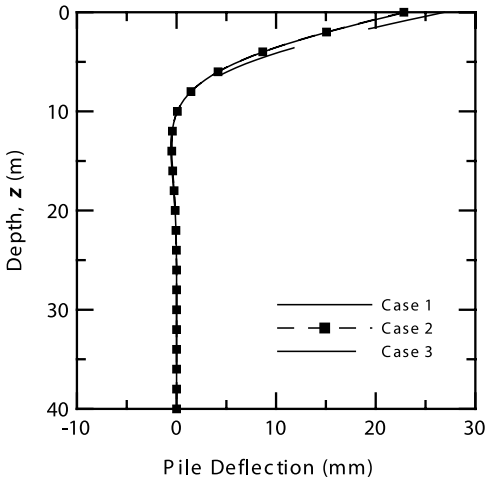

Fig. 9. Effect of varying soil modulus in front and back of a 40-m long pile on its lateral response: for case 1, the soil modulus is the same in the front and back of pile; for case 2, in the top 4 m, the soil modulus increases by 50% from the *in situ* value in the front of the pile and decreases by 50% from the *in situ* value at the back of the pile; for case 3, in the top 4 m, the soil modulus increases by 50% from the *in situ* value in front of the pile and the soil loses contact with the pile at the back.

4. Conclusions

A new method of analysis for a single, circular pile embedded in a multi-layered elastic medium and subjected to a horizontal force and a moment at the head is presented. The solution is fast and produces results comparable to three-dimensional finite element analysis. Using this method, pile deflection, slope of the deflection curve, bending moment and shear force for the entire length of the pile can be obtained if the following are known: the pile radius and length, thicknesses of the soil layers, Young's modulus of the pile material, the elastic constants of the soil in the various layers, and the magnitudes of the applied force and moment.

The governing differential equation for pile deflection is obtained using the principle of minimum potential energy, and closed-form solutions are obtained for this differential equation. The differential equations for the soil displacements also follow from the principle of minimum potential energy and are formulated through finite difference representations of the derivatives. The differential equations of pile and soil displacements are interdependent, thus an iterative scheme was required to solve the equations simultaneously.

The analysis is quite flexible, allowing variation of soil modulus in every direction — radial, circumferential or vertical. Illustrations of use of the analysis for layered soils show that the variation of soil properties in the horizontal direction has a definite impact on pile response. We have illustrated this through examples in which the soil Young's modulus varied radially (such as could happen due to disturbance) and circumferentially. Circumferential variation can be used to account for the impact of load direction on the state of the soil around the pile and for lack of contact between the pile and soil behind the pile, for example.

Acknowledgement

This material is based upon work supported by the National Science Foundation under Grant No. 0556347.

References

[1] Brown DA, Hidden SA, Zhang S. Determination of *p-y* curves using inclinometer data. Geotech. Testing J 1994;17(2):150-158.
[2] Cox WR, Reese LC, Grubbs BR. Field testing of laterally loaded piles in sand. Proc 6th Offshore Tech Conf Houston Texas 1974;2:459-472.
[3] Reese LC, Van Impe WF. Single piles and pile groups under lateral loading. A.A. Balkema, Rotterdam, Netherlands. 2001.
[4] Reese LC, Cox WR, Koop FD. Analysis of laterally loaded piles in sand. Proc 6th Offshore Tech Conf Houston Texas 1974;2:473-483.
[5] Reese LC, Cox WR, Koop FD. Field testing and analysis of laterally loaded piles in stiff clay. Proc 7th Offshore Tech Conf Houston Texas 1975;2:671-690.

[6] Banerjee PK, Davies TG, et al. The behavior of axially and laterally loaded single piles embedded in nonhomogeneous soils. Geotechnique 1978;28(3):309-326.
[7] Budhu M, Davies TG. Analysis of laterally loaded piles in soft clays. J Geotech Engng Div Am Soc Civ Engrs 1988; 114(1):21-39.
[8] Klar A, Frydman S. Three-dimensional analysis of lateral pile response using two-dimensional explicit numerical scheme. J Geotech Geoenv Engng Am Soc Civ Engrs 2002;128(9):775-784.
[9] Poulos HG. Behavior of laterally loaded piles: I – single piles. J Soil Mech Fdn Div Am Soc Civ Engrs 1971a;97(SM5):711-731.
[10] Poulos HG. Behavior of laterally loaded piles: III – socketed piles. J Soil Mech Fdn Div Am Soc Civ Engrs 1971b;98(SM4):341-360.
[11] Trochanis AM, Bielak J, Christiano P. Three-dimensional nonlinear study of piles. J Geotech Engng Am Soc Civ Engrs 1991;117(3):429-447.
[12] Basu D, Salgado R, Prezzi M. A continuum-based model for analysis of laterally loaded piles in layered soils. Géotechnique 2009;59(2):127-140.
[13] Basu D. Analysis of laterally loaded piles in layered soil. Ph.D. Thesis 2006; Purdue University.
[14] Basu D, Salgado R. Elastic analysis of laterally-loaded pile in multi-layered soil. Geomechanics and Geoengineering. An International Journal 2007a;2(3):183-196.
[15] Basu D, Salgado R. Method of initial parameters for piles embedded in layered soils. Geomechanics and Geoengineering. An International Journal 2007b;2(4):281-294.